





Isotopic distributions of thermal-neutron-induced fission fragments of near-symmetric fission of $^{239,241}\text{Pu}$ determined using calorimetric low-temperature detectors

Santwana Dubey ^{1,2,*}, Artur Echler^{1,2}, Peter Egelhof^{1,2}, Patrick Grabitz^{1,2}, Werner Lauterfeld^{1,2}, Manfred Mutterer^{1,2,†}, Stefan Stolte ^{1,2}, Aurelien Blanc³, Ulli Köster ³, Olivier Serot⁴, Gregoire Kessedjian^{4,5}, Saskia Kraft-Bermuth^{6,‡}, Pascal Scholz⁶, Shawn Bishop⁷, Jose M. Gomez-Guzman ⁷ and Friedrich Gönnerwein⁸

¹Johannes Gutenberg Universität, Mainz, Germany

²GSI Helmholtzzentrum für Schwerionenforschung, Darmstadt, Germany

³Institut Laue Langevin, Grenoble, France

⁴CEA/DES/IRENE/DER/SPRC, Cadarache, France

⁵LPSC, Université Grenoble-Alpes, CNRS/IN2P3, Grenoble, France

⁶Justus Liebig Universität, Giessen, Germany

⁷Technische Universität München, Garching, Germany

⁸Eberhard Karls Universität, Tübingen, Germany



(Received 1 May 2021; accepted 31 August 2021; published 21 September 2021)

Isotopic distributions were measured for the light fragment group in the transition region from asymmetric to symmetric fission for thermal neutron induced fission of ^{239}Pu and ^{241}Pu using the novel technology of calorimetric low temperature detectors in combination with the passive absorber method. Nuclear charge distributions were determined for 24 masses in the range $A = 89$ to $A = 112$ for $^{241}\text{Pu}(n_{\text{th}}, f)$ for the first time with the LOHENGRIN mass spectrometer. Moving from asymmetric to symmetric fission, known data were supplemented for masses from $A = 110$ to $A = 112$ for $^{241}\text{Pu}(n_{\text{th}}, f)$ and from $A = 109$ to $A = 113$ for $^{239}\text{Pu}(n_{\text{th}}, f)$. The isotopic yields were used to evaluate the charge polarization ΔZ and the proton odd-even effect δp with emphasis on the borderline between asymmetric and symmetric fission. This highlighted a virtual shell effect near $Z = 44$ which mirrors the effect of the $Z = 50$ shell in the complementary heavy fragment group of the two Pu isotopes ($Z = 94$) studied.

DOI: [10.1103/PhysRevC.104.034621](https://doi.org/10.1103/PhysRevC.104.034621)

I. INTRODUCTION

Nuclear fission is a complex process and major advances in its understanding have often been driven by new experimental data, e.g., fission fragment yields. Examples are the discoveries of new fission modes which had not been predicted by theory before, such as the asymmetric fission of Hg isotopes [1] or a compact symmetric fission mode in Th [2]. In particular, the study of isotopic fission yields allows a very detailed insight into the sharing of nucleons between light and heavy fragments in binary fission.

A huge amount of data on fission yields has been collected by a worldwide scientific collaboration since first investigations in 1941 [3]. In particular, thermal-neutron-induced fission of actinides has been in the focus. However, not all actinides have been scrutinized in the same detail. In particular, experiments with shorter-lived target nuclides are challenging due to their high activity. For example ^{241}Pu ($T_{1/2} = 14.35\text{a}$) has a specific activity of 3.8 GBq/mg and only few direct yield measurements of $^{241}\text{Pu}(n_{\text{th}}, f)$ have been published so

far, e.g., by Dickens [4], Thierens *et al.* [5], and Schillebeeckx *et al.* [6].

$^{239}\text{Pu}(n_{\text{th}}, f)$ and, at higher burnup, also $^{241}\text{Pu}(n_{\text{th}}, f)$ play an important role in nuclear reactor fuel. Thus, these nuclei are in the scope of the JEFF evaluation program of fission yields [7]. This work is based on experimental data and fission models, including the nuclear charge repartition models. Today, the Z_p model of Wahl [8] is commonly used in the evaluation but the weakness is the important dependency on fractional independent yield¹ data. Uncertainties of the resulting fission product inventory are most pronounced outside the fission peaks, i.e., in the symmetric and far asymmetric fission regions [11]. Complementary experimental data including isotopic yields could reduce these ambiguities.

We note that low-energy fission of the compound nucleus ^{240}Pu is considered a benchmark reaction in many theoretical fission studies; see the review by Schunck and Robledo and references therein [12]. In theory the interplay between sym-

¹Independent yields describe the probability of formation, expressed in percent, of a fission product with mass number A and nuclear charge Z after prompt neutron emission and before radioactive decay [8]. Fractional independent yields describe the fractions of the different elements (nuclear charge Z) for a given mass A . The fractions add up to unity (100%) for every mass [9,10].

*Corresponding author: s.dubey@gsi.de

†Deceased.

‡Present address: TH Mittelhessen University of Applied Sciences, Giessen, Germany.

metric and asymmetric fission has been studied by inspecting the shape of the potential energy surface (PES) near the saddle point. Microscopic calculations have been performed, e.g., by Berger *et al.* [13], Goutte *et al.* [14], Möller *et al.* [15], and Lemaitre *et al.* [16]. The transition region from asymmetric to symmetric fission is of particular interest since there three main fission modes are contributing, according to Brosa *et al.* [17]: a symmetric mode (SL) and two asymmetric modes (StI) and (StII). The SL mode is understood in the classic liquid drop model (LDM) while for the modes StI and StII shell stabilizing effects in the fragments have to be invoked. Precise experimental data on isotopic yields as obtained in the present work can provide insight into the interplay between modes coming into view in the nuclear charge polarization ΔZ , i.e., a shift of the actual fragment charges, away from the Z/A ratio equal to that of the fissioning system, and in the odd-even effect of nuclear charge yields.

With LOHENGRIN as the basic instrument outstanding contributions to our knowledge of isotopic distributions $Y(A, Z)$ of fission fragments from actinides were made. The instrument separates recoiling fission fragments according to mass and kinetic energy with high resolution (typically $M/\Delta M > 400$ and $E/\Delta E > 100$) [18,19]. There is, however, a serious limitation. While mass and energy measurements are straightforward, the determination of nuclear charges Z is less evident. Two different methods have been applied, based either on energy loss of charged particles or on γ -ray spectrometry. In the first method the slowing down of fission fragments on their passage through matter is studied along the track. The shape of the stopping curve, called the Bragg curve, depends on fragment charge Z . For a given segment Δx along the track the energy ΔE lost is measured. Experimentally the segment Δx is realized as a gas section in an ionization chamber or as thin foils the fragments have to cross. Carbon foils were used by Lang *et al.* [20] whereas Quade *et al.* [21] introduced Parylene-C foils. This $\Delta E/\Delta x$ technique is called the absorber method. In a second complementary method the fission products are identified by their decay properties [10,22]. After complete stopping in matter the fragments decay by emitting a γ -ray spectrum characteristic for a given nuclide. Both methods have limitations. Unfortunately, in decades of research it has not been possible to resolve nuclear charges larger than $Z = 42$ at the LOHENGRIN facility of the Institut Laue-Langevin (ILL), Grenoble [23–26]. In particular, measurements of nuclear charges by the absorber method both, in symmetric fission and heavy fragment asymmetric fission, remained out of reach.

The starting point for the present study was a suggestion by the late Manfred Mutterer that with further improved technology it could be possible to push the absorber method in the light fragment group beyond $Z = 42$, thus coming closer to symmetric fission in (n_{th}, f) reactions with heavy actinide targets. In the present work, a new detection system of calorimetric low-temperature detectors (CLTDs) is used to measure at LOHENGRIN by the passive absorber method isotopic yields of fragments from thermal-neutron-induced fission reactions. The CLTDs determine the particle energy by measuring the temperature rise due to thermalization of the particle's kinetic energy in the detector [27,28].

Due to their principle of operation, which is independent of ionization processes, CLTDs provide a fundamental advantage over conventional ionization detectors, in particular for the spectroscopy of heavy ions at low energies [9,27–30]. When compared to conventional ionization detectors (solid-state or gaseous detectors), CLTDs have several advantages, such as more complete energy detection, a smaller energy gap of the detected quanta (phonons), and the absence of any entrance window or dead layer. This results in substantial improvements over conventional ionization detectors in basic detector properties, namely energy resolution, energy linearity, detection threshold, etc. The advantages of CLTDs together with the use of high-quality absorber foils made from SiN with regard to homogeneity and energy loss straggling allow one to measure isotopic yields also for masses in symmetric fission and in the heavy mass region of the fission fragments, as shown by Dubey *et al.* [31,32]. In comparison, when using conventional ionization detectors with the passive absorber method, the limited nuclear charge resolution and the limited energy linearity for heavier fission fragments allow only isotopic yield measurements in the light fragment group for thermal-neutron-induced fission of actinides [24].

It is of great physics interest to push measurements towards the symmetric mass region, e.g., in order to study significant nuclear charge polarizations ΔZ not predicted by the LDM or odd-even effects in the nuclear charge yields. It is evident from cross section data and, perhaps even more directly, from mass distributions as a function of excitation energy of the fissioning compound that asymmetric and symmetric fission are two distinct fission modes. In the review *The Nuclear Fission Process* edited by Wagemans [33] there are numerous examples of mass distributions for neutron-induced fission of actinides as a function of neutron energy, demonstrating the distinct energy dependences of asymmetric and symmetric fission. It is so far conjectured from structures in the mass yield curves that, in contrast to asymmetric fission, only a small odd-even effect in the charge yields should be present in symmetric fission. However, on the way from asymmetry to symmetry, LOHENGRIN experiments point to the onset of a sizable odd-even effect [20,34,35] right at the turnover from asymmetry to symmetry. Extending the nuclear charge yield measurements in the light fragment group by few more masses towards symmetry would hence allow noteworthy progress in confirming (or rejecting) the onset of a pronounced even-odd effect.

In the present work isotopic yields for $^{241}\text{Pu}(n_{\text{th}}, f)$ have been studied with high resolution at the LOHENGRIN recoil spectrometer of the Institut Laue-Langevin in Grenoble, covering the light mass range from asymmetric up to symmetric fission ($A = 89$ to $A = 112$). Moreover, prior data on $^{239}\text{Pu}(n_{\text{th}}, f)$ by Schmitt *et al.* [35] have been extended further towards symmetry ($A = 109$ to $A = 113$). This allows a direct comparison of yield features between the two fissioning systems.

II. EXPERIMENTAL SETUP

The experiment reported in this work was performed at the LOHENGRIN spectrometer installed at the ILL high

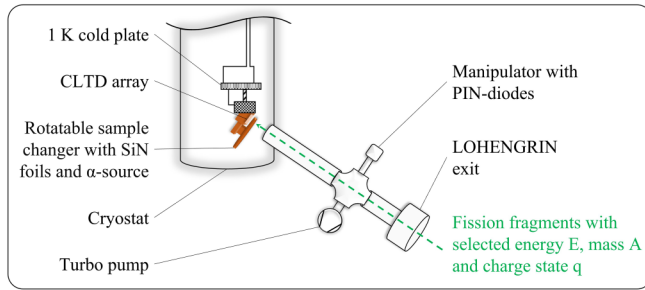


FIG. 1. Schematic of the experimental setup for isotopic yield measurements at the LOHENGRIN spectrometer.

flux reactor. Fission fragments from thermal-neutron-induced fission leave the target with small energy loss as charged ions and enter the LOHENGRIN spectrometer. It is a parabola mass spectrometer consisting of a horizontally deflecting homogeneous magnetic sector field and a vertically deflecting cylindrical condenser resulting in separation of the ionized fission fragments with respect to their mass over ionic charge, A/q , and velocity v , respectively, thus also defining a fixed ratio of kinetic energy to ionic charge, E/q . For the nuclear charge identification of the mass and energy separated fission fragments, we implement the passive absorber method [20] with the CLTDs measuring the residual energy after passage through SiN absorber foils. A schematic of the experimental setup is shown in Fig. 1 (details can be found in [9,36]). The CLTD array is operated under vacuum inside a ^4He -bath cryostat which is coupled to the straight exit flange of the LOHENGRIN spectrometer. The fragment beam is inclined by 35° . A remotely controlled piezo-driven sample changer for SiN absorber foils with different thicknesses (1, 5, 6, and $7\ \mu\text{m}$) is positioned inside the cryostat at a distance of a few millimeters to the CLTD array. A weak ^{241}Am α source is also mounted on the sample changer for calibration purposes. In addition, a movable manipulator was installed at a distance of 95 cm from the CLTD array with complementary PIN-diode detectors and additional SiN foils mounted on it.

In this work two fissile targets of highly enriched ^{239}Pu (99.98%) and ^{241}Pu (71.1%) were used, both in the form of oxide deposits on thick titanium backings. For each target the effective area visible by the LOHENGRIN spectrometer was constrained by a thick titanium diaphragm mounted on top of the target. The ^{239}Pu target had an effective area of $4 \times 0.35\ \text{cm}^2$, was $38\ \mu\text{g}/\text{cm}^2$ thick, and was covered by a $0.25\ \mu\text{m}$ thick Ni foil. The ^{241}Pu target had an effective area of $7 \times 0.5\ \text{cm}^2$, was $24\ \mu\text{g}/\text{cm}^2$ thick, and was covered by a $0.25\ \mu\text{m}$ thick Ni foil. For the ^{239}Pu target $>99.9\%$ of the fission rate represents $^{239}\text{Pu}(n_{\text{th}}, f)$ reactions while for the ^{241}Pu target 98.9% of the fission rate is from $^{241}\text{Pu}(n_{\text{th}}, f)$ reactions, the remainder being fission of $^{243}\text{Am}^*$ produced by double neutron capture on the beta decay product ^{241}Am .

The fission fragments undergo energy loss in the target and the cover of the target before they pass through the LOHENGRIN spectrometer. The original kinetic energies E of the fission fragments are therefore derived by calculating this energy loss in the target and its cover and adding it to the LOHENGRIN energy setting E_L . The energy loss calculated

TABLE I. List of measurements for $^{241}\text{Pu}(n_{\text{th}}, f)$ at different LOHENGRIN energies E_L and ionic charge states q .

$^{241}\text{Pu}(n_{\text{th}}, f)$					
A	$E_L(\text{MeV})$	q	A	$E_L(\text{MeV})$	q
89	94, 100	20	101	94, 100	22
90	94, 100, 106	20, 24	102	94, 100	23
91	94, 100	20	103	86, 94, 100	19, 22, 23
92	86, 94, 100, 106	21, 25	104	86, 94, 100	19, 23
93	94, 100	21	105	86, 94, 100	20, 23, 24
94	94, 100	21	106	86, 94, 100	20, 23, 24
95	94, 100	21	107	86, 94, 100	20, 23, 24
96	86, 94, 100	18, 21	108	86, 94, 100	20, 24, 25
97	94, 100	22	109	86, 94, 100	20, 24, 25
98	94, 100	22	110	86, 94, 100	20, 24, 25
99	94, 100	22	111	86, 94, 100	20, 24
100	94, 100	20, 22	112	86, 94, 100	21, 24, 25

in the target and the cover foil of the target was 6.7(1.9) MeV for $^{239}\text{Pu}(n_{\text{th}}, f)$ and 6.3(2.0) MeV for $^{241}\text{Pu}(n_{\text{th}}, f)$.

III. MEASUREMENTS AND DATA ANALYSIS

For the isotopic yield determination, a series of measurements was performed for masses from the light fragment region towards the symmetry region for $^{241}\text{Pu}(n_{\text{th}}, f)$ and $^{239}\text{Pu}(n_{\text{th}}, f)$ [37]. All measurements were performed with a $4\ \mu\text{m}$ thick SiN degrader foil stack as passive energy absorber on the disk installed inside the cryostat. The lists of measurements performed at different LOHENGRIN energies E_L and ionic charge states q for $^{241}\text{Pu}(n_{\text{th}}, f)$ and $^{239}\text{Pu}(n_{\text{th}}, f)$ are displayed in the Tables I and II.

The nuclear charge distributions of fission fragments are determined by measuring with the CLTDs the residual energy spectra of mass and energy separated fragments from the LOHENGRIN spectrometer after passing through SiN foils. Due to the energy loss dependence, different nuclear charges are separated. As an example, a spectrum measured with the CLTDs for mass $A = 108$ with the different Z contributions is shown in Fig. 2. The spectrum is fitted with a sum of Gaussians to determine the relative yields for the different nuclear charges corresponding to the individual Gaussian peaks shown in different colors in Fig. 2. We underline that for all studied cases the residual energy spectra could be well fitted

TABLE II. List of measurements for $^{239}\text{Pu}(n_{\text{th}}, f)$ at different LOHENGRIN energies E_L and ionic charge states q .

$^{239}\text{Pu}(n_{\text{th}}, f)$		
A	$E_L(\text{MeV})$	q
109	80, 84, 90, 94, 98	20, 24
110	80, 84, 90, 94, 98	20, 24
111	84, 90, 94	20, 24
112	80, 90	20
113	86	21

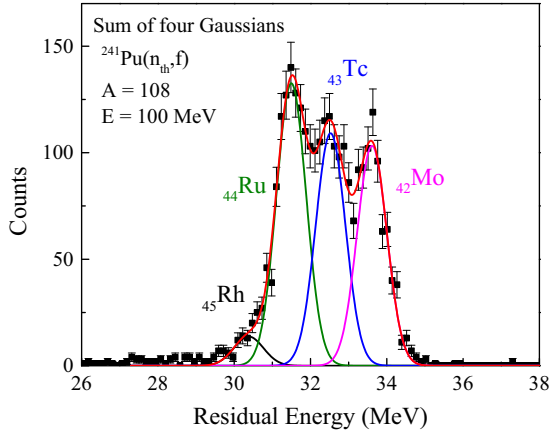


FIG. 2. Example spectrum measured with the CLTDs for mass $A = 108$ with different Z contributions in different colors. Note the leading contribution for the second peak at charge $Z = 44$, element ruthenium. The data were taken for 1.8 hours at an energy $E_L = 100$ MeV and an ionic charge state $q = 20$ with a $6 \mu\text{m}$ thick SiN energy degrader.

with symmetric Gaussians without tails; see also spectra in [9,36].

A systematic approach was followed for the measurements with the $^{241}\text{Pu}(n_{\text{th}}, f)$ target. With the aim to establish a reliable Z identification, masses $A = 89$ to 112 in series were measured with the same energy settings of LOHENGRIN, E_L , and with the same thickness of SiN degrader foils ($4 \mu\text{m}$ thick). This provided a very consistent Z -identification technique based on the energy loss dependence on mass and nuclear charge as shown in Fig. 3 (details in [9]). The second Z peak mentioned in the Fig. 3 caption was chosen as it is usually the central peak with relatively higher intensity,

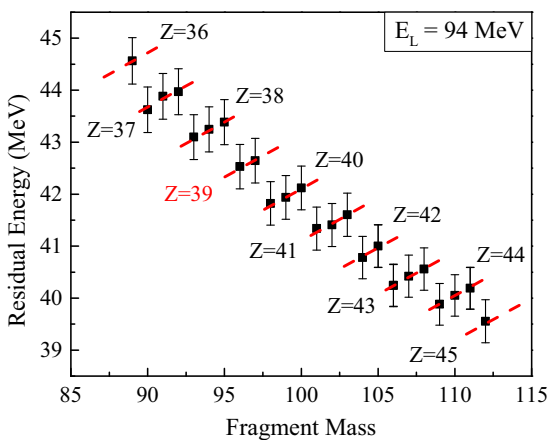


FIG. 3. Z -identification plot. The peak position of the second Z peak from the low-energy side of the residual energy spectra (e.g., Ru in the case of Fig. 2) measured with the CLTDs is plotted versus mass. Each mass in the range $89 \leq A \leq 112$ for $^{241}\text{Pu}(n_{\text{th}}, f)$ was measured at the LOHENGRIN energy setting $E_L = 94$ MeV with a $4 \mu\text{m}$ thick SiN foil stack. Each red line corresponds to a unique nuclear charge Z . $Z = 39$ marked in red was identified from the known Z -yield distributions for mass $A = 96$.

making it a good choice for systematic studies. The data points on the red dashed lines correspond to the fragments with the same nuclear charge but different mass number. Figure 3 is in addition a clear representation of the different scales of energy loss dependence on (a) the ion mass and (b) the nuclear charge. A weaker dependence of energy loss on ion mass as compared to the dependence on the nuclear charge is observed as expected [25]. On average, the energy separation between adjacent masses with the same nuclear charge is about 150 keV, whereas the energy separation between fragments of adjacent nuclear charges but the same mass is about 750 keV (see Fig. 3). These values were also confirmed by semiempirical calculations for the energy loss [9]. It should be noted here that this is due to the good energy linearity of the CLTDs, which makes it possible for such a Z -identification procedure to work. Unlike conventional detectors, where these systematics in energy loss cannot be observed due to the pulse height defects in the detectors, CLTDs offer an energy detection not affected by pulse height defects, and therefore allow one to exploit the nature of energy loss for the Z identification.

In the fits of the residual energy spectra measured with CLTDs (e.g., Fig. 2) the individual peak areas divided by the sum of the peak areas in the spectrum provide directly the nuclear charge distributions for given masses, ionic charge states, and kinetic energies selected by the LOHENGRIN spectrometer. The uncertainty is statistical, given by the fit error. Such data are presented in Table VII in the Appendix. The individual measurements are convoluted with ionic charge and kinetic energy distributions of the respective masses measured with the PIN diode to determine the ionic charge and kinetic energy distributions of the corresponding nuclear charges, denoted by $Y(A, Z, q_i, E_j)$. The fractional independent yields which correspond to the integral over the ionic charge and the kinetic energy distributions are approximated and evaluated by the following formula [9,10,38]:

$$Y(A, Z) = \frac{\int_E Y(A, Z, \bar{q}, E) dE \times \sum_i Y(A, Z, q_i, \bar{E})}{Y(A, Z, \bar{q}, \bar{E})} \quad (1)$$

where \bar{E} and \bar{q} represent the mean kinetic energy and the mean ionic charge for mass A . The quantities $\int_E Y(A, Z, \bar{q}, E) dE$ and $\sum_i Y(A, Z, q_i, \bar{E})$ are determined from the values of the integral of kinetic energy distributions fitted with exponentially modified Gaussian functions, and the sum of the ionic charge distributions, respectively. Independent yields are determined by multiplying the fractional independent yields with the mass yields determined with the PIN diode, and normalized to the mass yields from Schillebeeckx *et al.* [6] for $^{241}\text{Pu}(n_{\text{th}}, f)$ and to the mass yields from Schmitt *et al.* [35] for $^{239}\text{Pu}(n_{\text{th}}, f)$. We note that high accuracy mass yield measurements have been performed recently for $^{241}\text{Pu}(n_{\text{th}}, f)$ at the LOHENGRIN spectrometer [39,40]. Combined with the present nuclear charge distributions this will lead to a new and independent set of isotopic yields for $^{241}\text{Pu}(n, f)$ measured with the same instrument.

In addition, the standard corrections (for details see [9]) for the isotopic yield determination using CLTDs were implemented. These included the correction for the energy acceptance of the LOHENGRIN spectrometer. To correct for

TABLE III. Fractional independent yields in % for $^{241}\text{Pu}(n_{\text{th}}, f)$ obtained from the present experiment and derived first (\bar{Z}) and second (σ_Z) moments of the nuclear charge distributions per mass in the last two columns. The uncertainties include statistical and systematical errors.

Fractional independent yields (%) for $^{241}\text{Pu}(n_{\text{th}}, f)$										
Mass	Z = 34	Z = 35	Z = 36	Z = 37	Z = 38	Z = 39	Z = 40	Z = 41	\bar{Z}	σ_Z
89	2.9(0.6)	48.7(2.4)	44.0(2.2)	4.3(0.7)					35.497(34)	0.628(20)
90		7.6(3.8)	75.9(8.2)	15.7(7.3)	0.8(1.5)				36.096(118)	0.506(72)
91		2.9(0.6)	54.2(2.7)	40.1(2.0)	2.8(0.5)				36.429(34)	0.599(19)
92			25.3(1.9)	56.1(4.3)	18.5(2.0)				36.932(51)	0.659(26)
93			7.0(1.4)	58.6(2.9)	33.6(1.7)	0.7(0.1)			37.281(36)	0.597(22)
94			2.5(0.5)	28.5(1.4)	65.4(3.3)	3.5(0.6)			37.700(37)	0.575(19)
95			0.3(0.1)	13.5(0.7)	74.1(3.8)	12.1(2.1)			37.981(44)	0.517(19)
96				3.9(0.6)	55.5(2.8)	35.1(3.1)	5.5(1.2)		38.422(44)	0.659(28)
97				1.5(0.3)	38.4(1.9)	52.7(2.7)	7.3(1.2)		38.658(35)	0.634(22)
98					20.7(4.1)	53.5(2.6)	23.8(1.2)	2.0(0.3)	39.071(50)	0.721(35)
99					3.4(0.7)	52.7(2.6)	40.2(2.1)	3.7(0.6)	39.442(34)	0.623(20)
100					0.1(0.0)	15.4(0.8)	74.8(3.8)	9.7(1.6)	38.658(42)	0.502(18)
Mass	Z = 39	Z = 40	Z = 41	Z = 42	Z = 43	Z = 44	Z = 45	Z = 46	\bar{Z}	σ_Z
101	7.7(1.5)	62.4(3.1)	27.2(1.4)	2.7(0.5)					40.248(37)	0.628(22)
102	0.7(0.1)	44.5(2.2)	48.8(2.5)	6.0(1.0)					40.601(35)	0.612(21)
103		14.1(2.2)	56.5(4.0)	29.4(2.9)					41.154(54)	0.641(31)
104		4.2(1.3)	35.7(3.6)	55.5(4.8)	4.6(1.2)				41.605(63)	0.645(37)
105		0.4(0.3)	22.1(2.5)	65.0(3.9)	12.6(1.8)				41.896(50)	0.594(26)
106			5.5(1.3)	66.9(4.8)	25.0(2.1)	2.6(0.8)			42.246(54)	0.589(29)
107				29.6(3.0)	56.1(3.5)	14.3(3.3)			42.847(57)	0.644(37)
108				23.3(6.6)	50.7(3.3)	26.0(3.7)			43.027(81)	0.702(57)
109				3.4(1.7)	42.1(4.1)	50.9(4.6)	3.6(1.3)		43.548(65)	0.623(42)
110					20.3(2.3)	71.7(3.7)	8.0(1.6)		43.876(47)	0.517(23)
111					7.8(1.8)	79.7(4.1)	12.6(2.2)		44.048(50)	0.448(24)
112					3.4(1.8)	79.6(4.8)	12.3(3.2)	4.7(1.6)	44.183(63)	0.559(46)

this effect, count rates of each measurement are divided by the energy set at the LOHENGRIN spectrometer for normalization because the accepted energy range is proportional to the chosen energy for the LOHENGRIN settings. A further correction for target burn-up was accounted for by regularly monitoring the decrease in fission rate of a reference mass. The target burn-up curve thus obtained is described with an exponential decay curve and corresponding corrections are applied in the yield calculations.

Finally let us note a caveat resulting from the measurement strategy: all isotopic yield measurements at mass- and energy-selective spectrometers, like LOHENGRIN or HIAWATHA [41], have to be summed over spectrometer settings covering multiple kinetic energies E and ionic charge states q to determine fractional independent yields $Y(A, Z)$. In a previous paper [36] we focused on an accurate measurement of only two masses ($A = 92$ and $A = 96$) with a very detailed investigation of the influence of E and q settings on the yields. Here the focus is opposite, namely to obtain for $^{241}\text{Pu}(n_{\text{th}}, f)$ and $^{239}\text{Pu}(n_{\text{th}}, f)$ valid nuclear charge yields with measurements at only few kinetic energies and ionic charge states in the light mass peak, and in the transition from asymmetric to symmetric fission. To enable a direct comparison of peak positions of neighboring masses in Fig. 3, experiments have been deliberately performed at fixed kinetic energies for a wide range of masses. However, in reality the average fragment kinetic energies will slightly vary over the mass ranges, e.g.,

by ± 1 MeV between $A = 89$ and $A = 109$ in $^{239}\text{Pu}(n_{\text{th}}, f)$ [35]. Hence, the measurements at fixed energies will sample slightly different parts of the kinetic energy distribution for different masses. Therefore, the present data should not be overinterpreted in terms of possible fine structures of the kinetic energy distribution or correlations of isotopic yields and kinetic energy.

IV. RESULTS

The results for the isotopic yields $Y(A, Z)$ determined for the two reactions $^{241}\text{Pu}(n_{\text{th}}, f)$ and $^{239}\text{Pu}(n_{\text{th}}, f)$ investigated in the present work are displayed in Figs. 4 and 5, and in numerical form in Tables III–VII. The errors reported for the isotopic yields are the total uncertainties with contributions from statistical and systematic uncertainties as discussed in [9,36]. The systematic uncertainties dominate for all but the heaviest measured mass ($A = 112$ for ^{241}Pu and $A = 113$ for ^{239}Pu). We note that some of these systematic uncertainties, namely a possible bias due to the chosen ionic charge or kinetic energy settings on the fractional independent yields [36], could be reduced by additional measurements at more q and E settings. The values of the independent yields include moreover the normalization uncertainty of the available mass yields [6,35]. For $^{241}\text{Pu}(n_{\text{th}}, f)$ new mass yields with higher accuracy will become available in future [39,40]. The nuclear charge distributions measured at specific kinetic energies and

TABLE IV. Independent yields in % for $^{241}\text{Pu}(n_{\text{th}}, f)$ obtained from multiplying the fractional independent yields of Table III with mass yields from Ref. [6] shown in the last column. The uncertainties include statistical and systematic errors but no covariance data.

Independent yields (%) for $^{241}\text{Pu}(n_{\text{th}}, f)$									
Mass	Z = 34	Z = 35	Z = 36	Z = 37	Z = 38	Z = 39	Z = 40	Z = 41	Mass yield (%)
89	0.04(1)	0.70(4)	0.63(4)	0.06(1)					1.4(1)
90		0.13(7)	1.33(15)	0.27(13)	0.014(27)				1.8(1)
91		0.06(1)	1.12(6)	0.83(5)	0.06(1)				2.1(1)
92			0.61(5)	1.35(11)	0.45(5)				2.4(1)
93			0.21(4)	1.76(10)	1.01(6)	0.021(4)			3.0(1)
94			0.09(2)	1.04(6)	2.39(13)	0.13(2)			3.7(1)
95			0.011(2)	0.56(3)	3.07(17)	0.50(9)			4.1(1)
96				0.17(3)	2.45(13)	1.55(14)	0.25(5)		4.4(1)
97				0.08(2)	1.87(10)	2.57(14)	0.36(6)		4.9(1)
98					1.05(21)	2.71(14)	1.20(7)	0.10(2)	5.1(1)
99					0.20(4)	3.07(16)	2.35(13)	0.22(4)	5.8(1)
100					0.006(1)	0.97(5)	4.71(25)	0.61(10)	6.3(1)
Mass	Z = 39	Z = 40	Z = 41	Z = 42	Z = 43	Z = 44	Z = 45	Z = 46	
101	0.50(10)	4.06(21)	1.77(10)	0.17(3)					6.5(1)
102	0.05(1)	2.98(16)	3.27(18)	0.41(7)					6.7(1)
103		0.97(15)	3.91(29)	2.04(20)					6.9(1)
104		0.29(9)	2.50(26)	3.87(34)	0.32(9)				7.0(1)
105		0.03(2)	1.46(17)	4.29(27)	0.83(12)				6.6(1)
106			0.32(8)	3.89(29)	1.45(12)	0.15(5)			5.8(1)
107				1.38(14)	2.62(17)	0.67(15)			4.7(1)
108				0.78(22)	1.69(12)	0.87(12)			3.3(1)
109				0.08(4)	0.93(9)	1.12(11)	0.08(3)		2.2(1)
110					0.25(3)	0.87(6)	0.10(2)		1.2(1)
111					0.04(1)	0.43(3)	0.07(1)		0.53(3)
112					0.007(4)	0.17(2)	0.026(7)	0.010(4)	0.21(2)

ionic charge states [9] are listed in Table VII in the Appendix. These individual data have the highest accuracy as they do not suffer from the systematic uncertainties related to the averaging process.

The statistical error including the fit error was determined using the ORIGINLAB software for each residual energy spectrum measured with the CLTDs. Additionally, an error of less than 0.6% was estimated due to the thermal neutron flux instability [10]. The systematic uncertainty due to the approximation used for fractional independent yield calculations [see Eq. (1)] leads to an error of less than 1.3% (see also [9,10]). Additional errors propagate from the errors in mass yields used to determine the independent yields from the fractional independent yields.

For $^{241}\text{Pu}(n_{\text{th}}, f)$, data for 24 masses from $A = 89$ to $A = 112$ were measured for different energy and ionic charge state settings. For $^{239}\text{Pu}(n_{\text{th}}, f)$, data for five masses towards the symmetry region were measured from $A = 109$ to $A = 113$ at different energies and ionic charge states. Results for the fractional independent and independent yields obtained from the present experiment for thermal neutron induced fission of ^{241}Pu are plotted in Fig. 4 versus the atomic mass. The data points with the same color correspond to a particular nuclear charge as marked on the plot with the same color. The lines passing through the data points in Fig. 4 show the trend for individual nuclear charges. Similarly the yields obtained in the present experiment are plotted for thermal neutron induced fission of ^{239}Pu with solid data points in Fig. 5. The isotopic

TABLE V. Fractional independent yields in % for $^{239}\text{Pu}(n_{\text{th}}, f)$ obtained from the present experiment and derived first (\bar{Z}) and second (σ_Z) moments of the nuclear charge distributions per mass in the last two columns. The uncertainties include statistical and systematic errors.

Fractional independent yields (%) for $^{239}\text{Pu}(n_{\text{th}}, f)$						
Mass	Z = 43	Z = 44	Z = 45	Z = 46	\bar{Z}	σ_Z
109	24.7(2.7)	68.6(5.2)	6.7(1.9)		43.820(62)	0.531(31)
110	1.7(0.9)	90.5(4.0)	7.8(1.8)		44.061(45)	0.303(19)
111	1.4(1.1)	72.2(4.4)	26.4(3.3)		44.250(56)	0.464(29)
112		39.8(6.6)	47.7(5.7)	12.5(5.0)	44.727(101)	0.669(70)
113			74.6(24.3)	25.4(12.9)	45.254(275)	0.435(125)

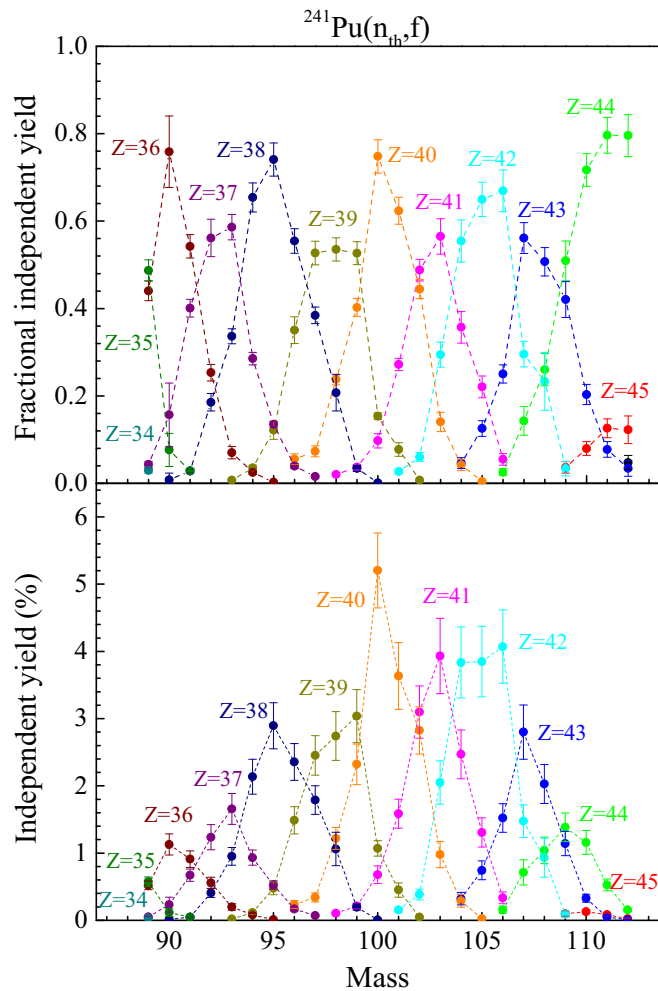


FIG. 4. Fractional independent yields (top) and independent yields (bottom), averaged over kinetic energies and ionic charge states, plotted for atomic masses $A = 89$ to 112 for $^{241}\text{Pu}(n_{\text{th}}, f)$ determined in the present work. The data points are connected with lines to show the trend.

yields measured in the present experiment are compared to previously published data and are found to be consistent with the available data in the literature from Schillebeecx *et al.* [6] for ^{241}Pu measured with the Cosi-Fan Tutte spectrometer for

TABLE VI. Independent yields in % for $^{239}\text{Pu}(n_{\text{th}}, f)$ obtained from multiplying the fractional independent yields of Table V with mass yields from Ref. [35] shown in the last column. The uncertainties include statistical and systematic errors but no covariance data.

Independent yields (%) for $^{239}\text{Pu}(n_{\text{th}}, f)$					
Mass	$Z = 43$	$Z = 44$	$Z = 45$	$Z = 46$	Mass yield (%)
109	0.26(3)	0.71(6)	0.07(2)		1.04(3)
110	0.01(1)	0.52(4)	0.05(1)		0.57(3)
111	0.003(3)	0.16(1)	0.06(1)		0.22(1)
112		0.044(8)	0.053(7)	0.014(6)	0.11(1)
113			0.056(26)	0.019(11)	0.075(24)

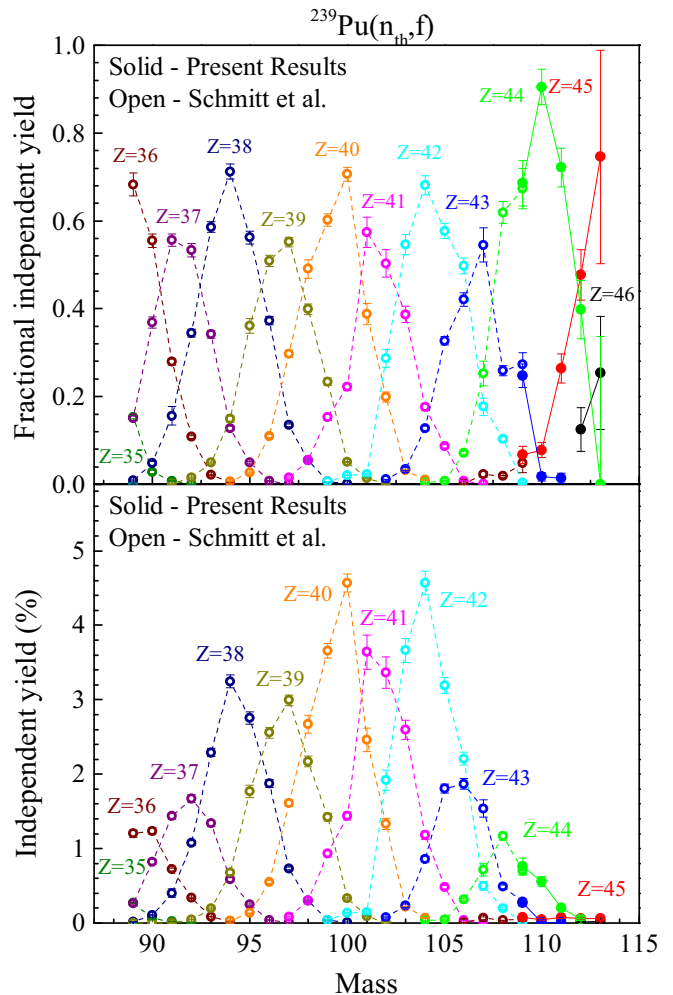


FIG. 5. Fractional independent yields (top) and independent yields (bottom), averaged over kinetic energies and ionic charge states, plotted for atomic masses $A = 89$ to 113 for $^{239}\text{Pu}(n_{\text{th}}, f)$. The solid dots for $A = 109$ to 113 correspond to the present results and the open dots to data from Schmitt *et al.* [35] for comparison. The data points are connected with lines to show the trend.

the three nuclear charges $Z = 39, 41$ and 43 (Fig. 6), and from Schmitt *et al.* [35] measured at LOHENGRIN for ^{239}Pu for mass $A = 109$ (plotted with open data points in Fig. 5). The agreement of the present results with measurements with completely different experimental setups [6,35] gives confidence in the methodology applied for the present investigations.

V. DISCUSSION

In the top part of Figs. 4 and 5 we observe the odd-even staggering in the fractional independent yields. The even Z -peaks are consistently higher compared to the odd Z -peaks. The evident reason for this staggering which enhances even charge splits is proton pairing in fragments from fission of even- Z compounds (plutonium with an even $Z = 94$ in this case). For thermal neutron induced fission a dominant odd-even effect is observed reflecting that the nuclear pairing effect plays a major role.

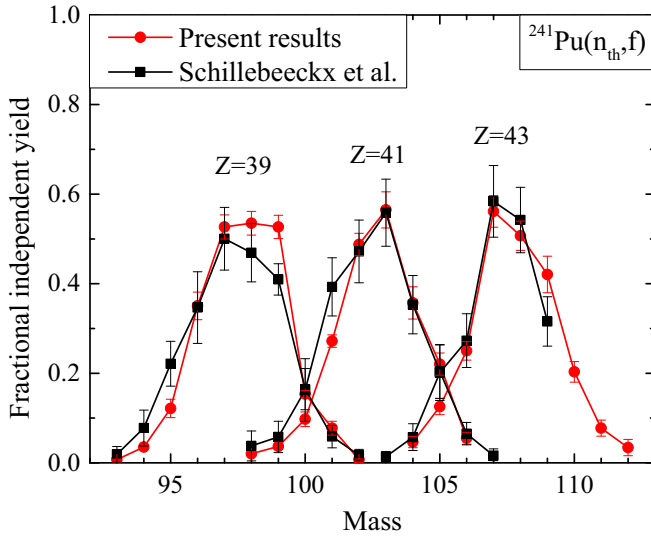


FIG. 6. Fractional independent yields for $Z = 39, 41, \text{ and } 43$ for $^{241}\text{Pu}(n_{\text{th}}, f)$ from the present work (red data points) in comparison with data from Schillebeeckx *et al.* [6] (black data points). The data points are connected with lines to show the trend.

However, since fission fragment yields vary as function of both, proton and neutron number of the respective fragments, subtle underlying structures may be less evident when regarding only these fractional independent or independent yields or summed mass or elemental yields respectively. Certain derived differential quantities are better suited for this purpose.

A key indicator of shell effects not foreseen in the LDM is the so-called charge polarization of fragments usually represented by ΔZ . The polarization ΔZ measures the deviation of the mean nuclear charge $\langle Z \rangle$ for fixed primary mass A'_L from an unchanged charge density (UCD). It is given by

$$\Delta Z = Z_{\text{UCD}} - \langle Z \rangle \quad \text{with } Z_{\text{UCD}} = (A'_L/A_F)Z_F. \quad (2)$$

Z_{UCD} is the unchanged charge distribution identical to the A_F/Z_F ratio of the fissioning nucleus and $\langle Z \rangle$ is the average value of the measured isobaric nuclear charge distribution integrated over the kinetic energy distribution. The quantity A'_L is the primary light fragment mass number before neutron evaporation found from $A'_L = A_L + \nu(A'_L)$ with A_L the mass number after neutron evaporation as measured in the present experiment, and $\nu(A'_L)$ the average number of neutrons emitted from the primary fission fragment. The masses for A'_L in $^{239}\text{Pu}(n_{\text{th}}, f)$ were determined using the most recent and accurate mass-dependent neutron emission data (“neutron sawtooth”) from Göök *et al.* [42]. As approximation the same data were also adopted for $^{241}\text{Pu}(n_{\text{th}}, f)$ since no experimental neutron sawtooth data are available for this system.

The charge polarizations ΔZ for the two reactions $^{241}\text{Pu}(n_{\text{th}}, f)$ and $^{239}\text{Pu}(n_{\text{th}}, f)$ are shown in Fig. 7 as a function of masses after and before neutron evaporation, A_L and A'_L , respectively. We note that the bottom scale A_L represents the accurate masses, measured with “perfect” mass resolution due to negligible cross-talk of neighboring masses in the LOHENGRIN spectrometer. However, the approximate pre-neutron mass scale A'_L on top has a larger uncertainty which

is dominated by the uncertainties of the experimental neutron sawtooth data. The experimental challenge to obtain accurate neutron sawtooth data outside the fission peaks is evident from the dispersion of results from different experiments, see Fig. 3 in [42] and Fig. 9 in [43].

The evaluation of ΔZ for $^{241}\text{Pu}(n_{\text{th}}, f)$ and $^{239}\text{Pu}(n_{\text{th}}, f)$ is based on the measured isotopic yield distributions shown in Fig. 4 for $^{241}\text{Pu}(n_{\text{th}}, f)$ and in Fig. 5 for $^{239}\text{Pu}(n_{\text{th}}, f)$. The modulations of ΔZ in Fig. 7 follow the same trend of systematically larger yields for even charges Z compared to odd charges. However, catching the eye in Fig. 7 for both plutonium isotopes ^{241}Pu and ^{239}Pu , are the steep surges of ΔZ for the light fragment charge $Z_L = 44$. This broad impact at charge $Z_L = 44$ in the light fragment group appears to mirror the importance of the complementary charge number $Z_H = 50$ in the heavy group for Pu with the charge of the fissioning compound $Z_F = 94$. It is recalled that nuclides close to the doubly magic ^{132}Sn play a key role in asymmetric fission. This most striking effect is not foreseen in the LDM but it is readily understood.

For complementary fragments, light L and heavy H, the following relations hold for the yields of primary masses A' and charges Z in binary fission of a compound nucleus F:

$$A_F = A'_L + A'_H = \text{const} \quad \text{and} \quad Z_F = Z_L + Z_H = \text{const}. \quad (3)$$

In a binary fission process the yields for the two fragments L and H are strictly equal:

$$Y(A'_L) = Y(A'_H) \quad \text{and} \quad Y(Z_L) = Y(Z_H). \quad (4)$$

The enhanced yields of the magic heavy fragments with $Z_H = 50$ (tin) thus impose the same enhanced yields in the light fragment for $Z_L = 44$ (ruthenium).

In the present experiment for the first time the stabilizing feature of the $Z_H = 50$ shell in the heavy fragment directly shows up like a mirror in the light group for two Pu-isotopes. The outstanding role of charge $Z_L = 44$ is seen in the fractional independent yields in Fig. 4 for $^{241}\text{Pu}(n_{\text{th}}, f)$ and in Fig. 5 for $^{239}\text{Pu}(n_{\text{th}}, f)$. For a primary mass near $A'_L = 112$ the contribution of $Z_L = 44$ comes close to 80%.

It should be stressed that there is no stabilizing shell effect known for nuclei with charge number $Z_L = 44$ nor for neutron numbers near $N = 66$. Only in binary fission with a complementary heavy fragment with the magic charge $Z_H = 50$ the conservation of nuclear charge in fission imposes a mirror effect in the yield of the complementary non-magic fragment with $Z_L = 44$.

But how the large yield of $Z_L = 44$ can produce such a huge effect in the charge polarization ΔZ in Fig. 7 remains a question still to be investigated in more detail.

Similar findings in the reaction $^{235}\text{U}(n_{\text{th}}, f)$ were noted by Clerc *et al.* [34] and Lang *et al.* [20] for the light fragment charge $Z_L = 42$ (molybdenum). For uranium the charge complementary to $Z_L = 42$ is in the heavy group again the magic $Z_H = 50$. Note that the compound charges Z_F for plutonium and uranium are 94 and 92 while the key charges Z_L for asymmetric fission in the light group are 44 and 42, respectively.

A further noteworthy phenomenon in low energy fission are charge odd-even effects in the isotopic yields as a function

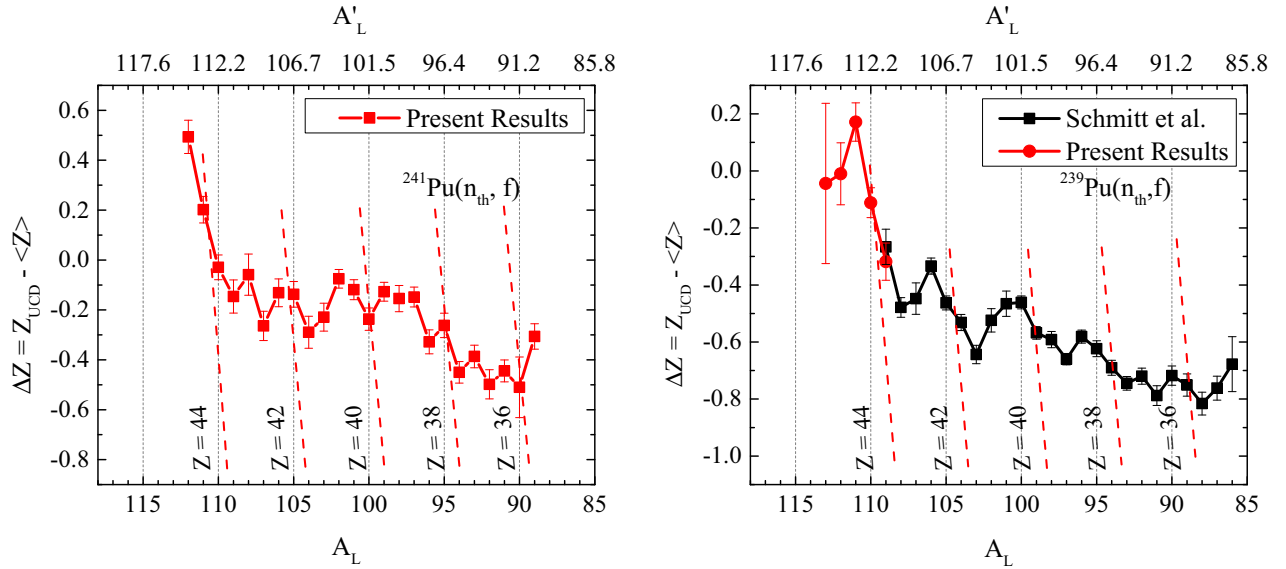


FIG. 7. Charge polarization ΔZ as a function of the secondary mass A_L in the light fragment group for $^{241}\text{Pu}(n_{\text{th}}, f)$ to the left and $^{239}\text{Pu}(n_{\text{th}}, f)$ to the right. The corresponding approximate primary masses A'_L are given on top of the graph (corresponding masses connected by vertical grey dashed lines), but these carry an inherent uncertainty due to the statistical nature of the neutron evaporation. For $^{239}\text{Pu}(n_{\text{th}}, f)$ the present results are combined with results of Schmitt *et al.* [35]. The dashed red lines mark the respective mean Z for corresponding masses. The data points are connected with lines to show the trend.

of the fragment mass A . In Fig. 4 for $^{241}\text{Pu}(n_{\text{th}}, f)$ and in Fig. 5 for $^{239}\text{Pu}(n_{\text{th}}, f)$ it is a general observation that the yields for even charges are larger than the yields for odd charges. The reason for this staggering with even charges being enhanced is proton pairing in fragments from fission of even- Z compounds. In the case of thermal neutron induced fission this odd-even effect is very pronounced bringing to evidence that nuclear pairing effects are important. The odd-even staggering in charge yields is therefore a critical test of theoretical calculations of pair-breaking in fission.

The global odd-even-effect for the protons in the full light fragment group was studied extensively experimentally in fission of actinides [33]. It is defined as

$$\Delta p = \frac{\sum Y(Z_e) - \sum Y(Z_o)}{\sum Y(Z_e) + \sum Y(Z_o)}, \quad (5)$$

where the yields for even Z and for odd Z fragment charges, $Y(Z_e)$ and $Y(Z_o)$, are summed over the full mass range of the light fragment mass group. Similarly to the case of the charge polarization ΔZ , more detailed insight into the fission process is obtained from the so-called local odd-even effect where the odd-even staggering is evaluated for a smaller mass range of fragments. Following the definition of a local neutron odd-even effect by Tracy *et al.* [44], Lang *et al.* [20] calculated the local proton odd-even effect δp based on a method of differences, given by

$$\delta p = \frac{1}{8}(-1)^{Z+1} \{[\ln Y(Z+3) - \ln Y(Z)] - 3[\ln Y(Z+2) - \ln Y(Z+1)]\}. \quad (6)$$

The natural logarithms of independent yields for four charges, Z , $Z+1$, $Z+2$, and $Z+3$, are employed. In the case of a

smooth Gaussian-like isotopic distribution there is no odd-even structure in the distribution. The above definition yields indeed $\delta p = 0$. A nonzero $\delta p \neq 0$ is taken as a measure of a local odd-even effect in the charge yields averaged over the four charges considered. The odd-even effect is attributed to the midpoint charge $\bar{Z} = (Z+1.5)$.

Lang *et al.* [20] applied this prescription to isotopic fission yields of $^{235}\text{U}(n_{\text{th}}, f)$ measured at LOHENGRIN and observed a significant rise of the proton odd-even effect δp at $Z = 42$ (or more precisely at $\bar{Z} = 41.5$). Previously Clerc *et al.* [34] had speculated that the rise of elemental yields at $Z = 42$ and the drop at $Z = 43$ could be related to the $Z = 50$ shell of the complementary fragment. More measurements, e.g., for fission of plutonium isotopes, were recommended to clarify this point.

Provided the above discussion of the charge polarization is generally valid, one should expect for Pu isotopes large odd-even effects at $Z = 50$ in the heavy fragment group and at $Z = 44$ in the light group. The present experiment confirms this expectation.

In the studies by Schmitt *et al.* [35] of the $^{239}\text{Pu}(n_{\text{th}}, f)$ reaction, besides the charge polarization ΔZ also the odd-even effect was evaluated. Results for the fission reaction of $^{239}\text{Pu}(n_{\text{th}}, f)$ complemented by our present results are plotted together with the data for $^{241}\text{Pu}(n_{\text{th}}, f)$ from the present experiment and in addition for $^{235}\text{U}(n_{\text{th}}, f)$ from Lang *et al.* [20] in one single figure. The data are shown in Fig. 8 as a function of the nuclear charge Z . It is obvious that the behavior of the δp distributions is similar for uranium and plutonium targets but shifted by two charges. At mid-charges there is first a minimum of the odd-even effect and then a maximum at the largest charges that could be analyzed. Remarkably the

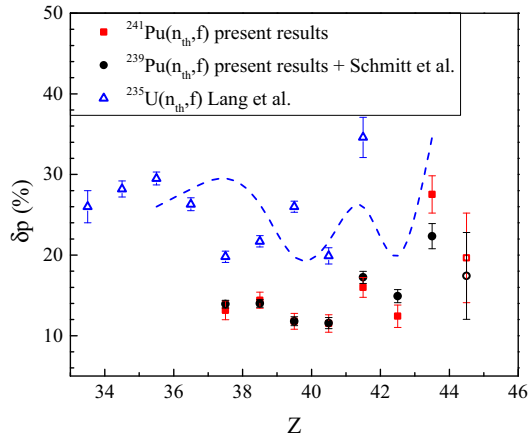


FIG. 8. Local proton odd-even effect δp versus the nuclear charge Z for the (n_{th}, f) reactions of ^{235}U (blue triangles), ^{239}Pu (black points) and ^{241}Pu (red squares). Results from the present experiment are displayed together with results from Schmitt *et al.* [35] and from Lang *et al.* [20]. We remind that δp is calculated as a third difference from the elemental yields of four consecutive nuclear charges (Z to $Z + 3$). δp is then plotted for the midpoint $Z + 1.5$. The last point at $Z = 44.5$ is plotted as open symbol to show that it carries an additional, not quantifiable, systematic uncertainty due to the contribution of nonmeasured masses ($A > 112$ for ^{241}Pu and $A > 113$ for ^{239}Pu) to the elemental yields of $Z > 44$. The dashed blue line corresponds to the ^{235}U data shifted by two nuclear charges towards the right.

maxima of δp are seen at $Z = 42$ for $^{236}\text{U}^*$ and at $Z = 44$ for both $^{240}\text{Pu}^*$ and $^{242}\text{Pu}^*$. With the definition of Eq. (6) for the local-effect δp , these charge numbers become $Z = 41.5$ and $Z = 43.5$, respectively.² Making use of the standard technique for Z identification, Schmitt *et al.* could not, however, check the predictions for the Pu isotopes due to difficulties in the identification of charges near $Z = 45$. Our present experiments have now overcome this technical limitation and allowed us to measure isotopic yields up to $Z = 46$. They clearly demonstrate the presence of shell effects in binary fission as previously indicated by yield evaluations of light and heavy fragments performed by Wahl [8,45]. We note that the proton odd-even effect is not fully understood theoretically [26]. Various models have been proposed [46–49], but these explanations predict a local proton odd-even effect that is monotonically dropping towards symmetry. This is in conflict with the present observations.

Comparing Fig. 7 for the charge polarization ΔZ and Fig. 8 for the local odd-even-effect δp it is evident that the surges for ΔZ and the spikes in the odd-even effect δp are found at the same charge number $Z = 42$ (molybdenum) for

²We remind that the preponderance of the $Z = 44$ yields is already manifested in Tables III and V and Figs. 4 and 5, and also is clearly visible from the reduced second moment when $\bar{Z} \approx 44$. Thus, the observation of the shell effect is robust and influenced neither by the choice of the particular third difference method nor by systematic uncertainties due to nonmeasured masses.

$^{235}\text{U}(n_{th}, f)$ and at the charge number $Z = 44$ (ruthenium) for $^{239}\text{Pu}(n_{th}, f)$ and $^{241}\text{Pu}(n_{th}, f)$. These singled out charge numbers in the light fragment group are both complementary to the magic $Z = 50$ (tin) in the heavy group. It is hence evident that both effects have as a common origin the shell effect in the heavy fragment for $Z = 50$. However, in the light group the complementary charges carry no genuine shell effect, so we see simply a virtual effect mirroring that of the heavy complement.

VI. CONCLUSIONS

Isotopic yield distributions were determined for light fragment masses close to the symmetry region for thermal-neutron-induced fission of ^{239}Pu and ^{241}Pu , applying the passive absorber method. Progress in nuclear charge resolution was achieved by making use of CLTDs for fragment detection and thin SiN foils as absorber. For the target ^{241}Pu the masses from $A = 89$ to $A = 112$ were measured for the first time with perfect mass resolution at the LOHENGRIN spectrometer. For the target ^{239}Pu previous measurements were extended from $A = 109$ to $A = 113$. The measured yields revealed a conspicuous surge of the charge polarization $\Delta Z = (Z_{\text{UCD}} - \langle Z \rangle)$ for $Z = 44$ while a pronounced spike in the local proton odd-even effect δp appeared near the same charge $Z = 44$. The charge $Z_L = 44$ in the light fragment group is complementary to the magic charge $Z_H = 50$ in the heavy group. Recalling that, in contrast to symmetric fission, shell stabilized fragments near the doubly magic nucleus ^{132}Sn are the root of asymmetric fission in the heavy fragment group as an independent fission mode, the present experiments prove the presence of a virtual shell-like effect in the light fragment group of fissioning Pu nuclei that mirrors the real shell effect of the complementary heavy fragment. This mirror effect is due to the equality of yields of complementary fragments in binary fission. Conservation of fragment charges allows one to observe this effect in the light fragment group. But beware: Other properties of fission fragments at scission-like fragment deformations and hence prompt neutron emission (see, e.g., [42]) are not mirrored.

ACKNOWLEDGMENTS

We would like to thank Norbert Laurens (ILL, Grenoble) for the technical support. We acknowledge the financial support from the DFG by Grant No. KR3721/1-1 and from BMBF by Grant No. 05P15RGFAA.

APPENDIX

Fractional independent yields determined for individual ionic charges and kinetic energies for $^{241}\text{Pu}(n_{th}, f)$ are given in Table VII.

TABLE VII. Fractional independent yields in % for $^{241}\text{Pu}(n_{\text{th}}, f)$ obtained from the present experiment with derived first (\bar{Z}) and second (σ_Z) moments of the nuclear charge distributions per mass. E_L and E_F refer to the LOHENGRIN energy setting, and the corresponding energy from fission,^a respectively. The estimated E_F has an uncertainty of ± 1.5 MeV.

A	q	E_L	E_F	$Z = 34$	$Z = 35$	$Z = 36$	$Z = 37$	$Z = 38$	$Z = 39$	\bar{Z}	σ_Z	
89	20	94	99	2.9(0.6)	48.7(1.8)	44.0(1.7)	4.3(0.7)			35.497(32)	0.628(19)	
89	20	100	105	3.2(0.6)	49.7(1.8)	41.1(1.6)	6.1(0.8)			35.501(33)	0.659(20)	
90	20	94	99		5.3(0.6)	80.3(1.8)	13.7(1.1)	0.7(0.3)		36.098(27)	0.458(13)	
90	20	94	100		7.5(1.0)	77.9(2.5)	13.5(1.4)	1.1(0.5)		36.082(37)	0.497(20)	
90	24	94	103		2.1(0.8)	24.3(1.9)	46.9(2.3)	26.8(1.9)		36.984(42)	0.770(29)	
90	20	100	105		6.6(0.8)	79.0(2.3)	13.2(1.3)	1.2(1.1)		36.091(36)	0.489(32)	
91	20	94	99		2.9(0.5)	54.2(1.8)	40.1(1.6)	2.8(0.5)		36.429(30)	0.599(17)	
91	20	100	105		3.9(1.2)	64.3(3.5)	28.8(2.5)	3(1.1)		36.309(55)	0.592(32)	
92	21	86	88			21.7(1.0)	60.2(1.3)	18.1(1.0)		36.964(23)	0.630(12)	
92	21	86	90			22.7(0.6)	55.6(0.8)	21.8(0.6)		36.991(14)	0.667(7)	
92	21	100	104			29.0(1.0)	56.5(1.2)	14.5(0.9)		36.855(21)	0.644(12)	
92	21	106	110			38.3(1.2)	52.5(1.2)	9.1(0.8)		36.708(22)	0.624(13)	
92	25	94	97			31.5(0.8)	49.2(0.9)	19.3(0.7)		36.878(16)	0.702(9)	
93	21	94	99			7.0(0.9)	58.6(2.0)	33.6(1.6)	0.7(0.4)	37.281(31)	0.597(18)	
93	21	100	104			6.7(1.3)	57.7(2.8)	32.7(2.3)	2.9(0.9)	37.317(45)	0.640(29)	
94	21	94	100			2.5(0.7)	28.5(1.7)	65.4(2.4)	3.5(0.8)	37.700(35)	0.575(21)	
94	21	100	104			3.6(0.8)	27.6(1.9)	66.0(2.8)	2.8(0.8)	37.681(40)	0.587(24)	
95	21	94	99			0.3(0.3)	13.5(1.3)	74.1(2.3)	12.1(1.2)	37.981(33)	0.517(17)	
95	21	100	104			0.5(0.6)	17.2(1.7)	71.1(2.7)	11.2(1.4)	37.930(39)	0.548(23)	
A	q	E_L	E_F	$Z = 37$	$Z = 38$	$Z = 39$	$Z = 40$	$Z = 41$	$Z = 42$	\bar{Z}	σ_Z	
96	18	94	98	3.7(0.3)	56.9(0.8)	35.1(0.7)	4.3(0.3)			38.400(13)	0.633(8)	
96	21	86	87	4.4(0.3)	56.2(0.9)	34.3(0.7)	5.0(0.4)			38.400(14)	0.655(10)	
97	22	94	99	1.5(0.5)	38.4(1.8)	52.7(2.0)	7.3(1.0)			38.658(31)	0.634(20)	
97	22	100	104	1.9(0.9)	44.6(2.1)	48.2(2.1)	5.3(1.0)			38.569(34)	0.625(24)	
98	22	94	100		20.7(1.6)	53.5(2.1)	23.8(1.7)	2.0(0.6)		39.071(34)	0.722(22)	
98	22	100	105		32.0(1.8)	55.6(2.0)	11.2(1.3)	1.1(0.5)		38.815(32)	0.666(22)	
99	22	94	99		3.4(0.6)	52.7(1.8)	40.2(1.5)	3.7(0.6)		39.442(26)	0.623(17)	
99	22	100	104		4.1(1.1)	60.0(3.1)	33.9(2.4)	2.0(0.9)		39.338(43)	0.589(28)	
100	22	94	100		0.1(0.3)	15.4(1.5)	74.8(2.5)	9.7(1.2)		39.942(32)	0.502(18)	
100	22	100	105		1.3(0.6)	23.1(1.9)	73.1(2.7)	2.4(0.7)		39.767(35)	0.504(21)	
101	22	94	99			7.7(1.0)	62.4(2.2)	27.2(1.6)	2.7(0.6)	40.248(29)	0.628(19)	
101	22	100	104			10.2(1.4)	65.3(2.8)	22.9(2.0)	1.7(0.7)	40.161(37)	0.610(24)	
102	23	94	100			0.7(0.5)	44.5(2.1)	48.8(2.1)	6.0(1.0)	40.601(31)	0.612(21)	
102	23	100	105			2.7(0.7)	62.7(2.3)	31.9(1.7)	2.7(0.8)	40.347(30)	0.579(21)	
103	19	94	98			0.8(0.7)	16.0(1.8)	72.8(3.1)	10.4(1.6)	40.928(38)	0.539(27)	
103	23	94	102			0.3(0.7)	9.1(2.1)	52.7(2.5)	37.9(3.0)	41.283(43)	0.634(38)	
A	q	E_L	E_F	$Z = 40$	$Z = 41$	$Z = 42$	$Z = 43$	$Z = 44$	$Z = 45$	$Z = 46$	\bar{Z}	σ_Z
103	22	94	100	17.8(2.5)	61.9(3.1)	20.3(2.4)					41.024(45)	0.617(32)
103	23	100	104	28.7(2.2)	58.7(2.9)	12.6(1.7)					40.838(40)	0.622(36)
103	23	86	90	6.7(1.6)	46(2.6)	44.3(2.7)	3.0(1.0)				41.436(39)	0.664(31)
104	23	86	90	1.3(1.1)	26.2(2.9)	66.1(4.3)	6.4(1.7)				41.776(51)	0.572(35)
104	19	94	98	7.1(1.4)	42.5(2.2)	47.2(2.5)	3.2(0.9)				41.465(35)	0.675(28)
104	23	94	100	4.5(0.9)	39.3(1.9)	51.9(2.2)	4.3(0.9)				41.561(29)	0.650(21)
104	23	100	105	10.1(1.9)	55.8(3.2)	31.8(2.6)	2.3(1.4)				41.263(45)	0.665(37)
105	23	86	90	0.02(0.6)	8.4(1.8)	66.0(2.8)	25.6(2.4)				42.172(37)	0.557(30)
105	20	94	98	0.9(0.7)	26.7(2)	65.4(2.8)	7.1(1.2)				41.786(34)	0.572(23)
105	23	94	99	0.9(0.5)	22.0(1.8)	65.3(2.5)	11.8(1.4)				41.881(30)	0.599(20)
105	23	100	104		36.3(2.3)	62.0(2.8)	1.8(1.0)				41.655(36)	0.511(28)
105	24	100	104	0.8(1.2)	35.1(2)	59.4(2.5)	4.6(1.0)				41.678(33)	0.572(30)
106	24	86	92		1.7(0.9)	33.2(2.6)	57.0(3.1)	8.2(1.7)			42.716(39)	0.633(30)
106	20	94	98		5.2(1.1)	77.2(3.3)	17.1(2.2)	0.6(0.6)			42.131(37)	0.478(24)
106	23	94	100		8.2(1.5)	62.3(3.3)	25.9(2.2)	3.6(1.1)			42.249(39)	0.651(29)
106	24	94	100		5.7(1.1)	51.5(2.4)	38.5(2.1)	4.3(1.1)			42.413(31)	0.665(25)
106	24	100	106	0.1(0.5)	8.7(1.3)	77.4(2.9)	13.9(1.7)				42.050(33)	0.476(24)

TABLE VII. (*Continued.*)

A	q	E_L	E_F	Z = 40	Z = 41	Z = 42	Z = 43	Z = 44	Z = 45	Z = 46	\bar{Z}	σ_Z
107	24	86	90			22.4(2.8)	62.2(3.0)	15.4(2.7)			42.930(42)	0.611(29)
107	20	94	98		5.3(1.4)	41.2(2.6)	45.5(2.7)	8.0(1.7)			42.563(38)	0.715(33)
107	23	94	100			27.3(2.8)	57.3(3.2)	15.3(2.5)			42.880(43)	0.642(29)
107	24	94	100			35.9(2.1)	56.7(2.2)	7.4(1.3)			42.715(29)	0.594(20)
107	24	100	104			56.7(3.0)	40.5(2.3)	2.8(1.1)			42.462(35)	0.553(25)
108	24	86	90			2.5(1.2)	69.5(3.3)	27.9(2.9)			43.254(39)	0.490(24)
108	20	94	98			35.9(2.0)	34.6(2.5)	29.4(1.9)			42.935(32)	0.806(22)
108	25	94	100			6.9(4.4)	67.5(6.2)	25.6(6.3)			43.187(84)	0.538(59)
108	24	94	100			8.0(1.6)	70.8(2.9)	21.1(2.2)			43.131(35)	0.524(21)
108	24	100	104			21.3(2.0)	65.2(2.6)	13.5(1.8)			42.922(32)	0.585(20)
108	20	100	110			30.8(2.0)	31.0(2.7)	38.3(2.1)			43.075(34)	0.827(24)
109	24	86	90			1.5(0.8)	27.7(2.4)	65.8(3.4)	5(1.2)		43.743(37)	0.566(27)
109	20	94	98			4.0(1.1)	53.6(2.7)	39.8(2.4)	2.5(0.9)		43.408(33)	0.610(26)
109	24	94	99			4.9(1.6)	39.2(2.8)	50.2(3.3)	5.8(1.7)		43.569(41)	0.677(37)
109	24	100	104			5.1(1.6)	44.5(2.6)	49.6(3.2)	0.9(1.1)		43.463(38)	0.606(33)
110	24	86	91				26.5(2.7)	61.3(2.8)	12.3(2.4)		43.858(37)	0.606(27)
110	25	94	99				47.1(3.3)	52.9(2.9)			43.529(38)	0.499(30)
110	20	94	99				5.6(2.1)	89.7(4.3)	4.7(1.8)		43.990(42)	0.320(25)
110	24	94	100				20.3(2.0)	71.7(2.8)	8.0(1.5)		43.876(31)	0.517(19)
110	24	100	105				20.9(2.6)	72.2(3.3)	6.9(1.7)		43.860(38)	0.508(24)
111	24	86	91				5.2(1.3)	78.1(3.3)	16.7(2.3)		44.115(35)	0.454(20)
111	20	94	98				6.0(1.0)	83.1(2.6)	10.8(1.3)		44.048(25)	0.408(14)
111	24	94	99				6.9(1.3)	84.4(3.1)	8.7(1.5)		44.018(30)	0.395(17)
111	24	100	105				12.7(2.1)	80.7(3.4)	6.6(2.0)		43.938(37)	0.435(23)
112	21	86	92					73.3(6.9)	23.6(4.4)	3.1(2.5)	44.298(70)	0.520(62)
112	24	94	98				7.3(3.0)	72.2(8.5)	20.5(5.6)		44.132(89)	0.510(87)
112	21	94	100				3.4(1.8)	79.6(3.7)	12.3(3.0)	4.7(1.6)	44.183(43)	0.559(42)
112	21	100	106				4.1(2.1)	81.1(6.3)	14.8(5.2)		44.107(68)	0.421(41)

^a E_F has been corrected for the energy loss in the target and target cover. The target evolves over time [50] and the correction is applied based on regular scans with the PIN diode.

- [1] A. N. Andreyev, J. Elseviers, M. Huyse, P. Van Duppen, S. Antalic, A. Barzakh, N. Bree, T. E. Cocolios, V. F. Comas, J. Diriken, D. Fedorov, V. Fedosseev, S. Franchoo, J. A. Heredia, O. Ivanov, U. Köster, B. A. Marsh, K. Nishio, R. D. Page, N. Patronis, M. Seliverstov, I. Tsekhanovich, P. Van den Bergh, J. Van De Walle, M. Venhart, S. Vermote, M. Veselsky, C. Wagemans, T. Ichikawa, A. Iwamoto, P. Möller, and A. J. Sierk, *Phys. Rev. Lett.* **105**, 252502 (2010).
- [2] A. Chatillon, J. Taïeb, H. Alvarez-Pol, L. Audouin, Y. Ayyad, G. Bélier, J. Benlliure, G. Boutoux, M. Caamaño, E. Casarejos, D. Cortina-Gil, A. Ebran, F. Farget, B. Fernández-Domínguez, T. Gorbina, L. Grente, A. Heinz, H. T. Johansson, B. Jurado, A. Kelić-Heil, N. Kurz, B. Laurent, J.-F. Martin, C. Nociforo, C. Paradela, E. Pellereau, S. Pietri, A. Prochazka, J. L. Rodríguez-Sánchez, D. Rossi, H. Simon, L. Tassan-Got, J. Vargas, B. Voss, and H. Weick, *Phys. Rev. Lett.* **124**, 202502 (2020).
- [3] H. L. Anderson, E. Fermi, and A. V. Grosse, *Phys. Rev.* **59**, 52 (1941).
- [4] J. K. Dickens, *Nucl. Sci. Eng.* **70**, 177 (1979).
- [5] H. Thierens, E. Jacobs, P. D'hondt, A. De Clercq, M. Piessens, and D. De Frenne, *Phys. Rev. C* **29**, 498 (1984).
- [6] P. Schillebeeckx *et al.*, *Nucl. Phys. A* **580**, 15 (1994).
- [7] A. J. M. Plompen *et al.*, *European Phys. J. A* **56**, 181 (2020).
- [8] A. C. Wahl, *At. Data Nucl. Data Tables* **39**, 1 (1988).
- [9] S. Dubey, Isotopic yield determination for thermal neutron induced fission of ²³⁵U, ²³⁹Pu and ²⁴¹Pu in the light, symmetry and heavy mass regions using calorimetric low temperature detectors, Ph.D. thesis, Johannes Gutenberg University Mainz, 2019.
- [10] A. Bail, O. Serot, L. Mathieu, O. Litaize, T. Materna, U. Köster, H. Faust, A. Letourneau, and S. Panebianco, *Phys. Rev. C* **84**, 034605 (2011).
- [11] D. da Cruz, D. Rochman, and A. Koning, *Nucl. Data Sheets* **118**, 531 (2014).
- [12] N. Schunck and L. M. Robledo, *Rep. Prog. Phys.* **79**, 116301 (2016).
- [13] J. Berger, M. Girod, and D. Gogny, *Nucl. Phys. A* **428**, 23 (1984).
- [14] H. Goutte, J. F. Berger, P. Casoli, and D. Gogny, *Phys. Rev. C* **71**, 024316 (2005).
- [15] P. Möller, D. G. Madland, A. J. Sierk, and A. Iwamoto, *Nature (London)* **409**, 785 (2001).
- [16] J.-F. Lemaître, S. Goriely, S. Hilaire, and J.-L. Sida, *Phys. Rev. C* **99**, 034612 (2019).
- [17] U. Brosa, S. Grossmann, and A. Müller, *Phys. Rep.* **197**, 167 (1990).
- [18] E. Moll *et al.*, *Nucl. Instrum. Methods* **123**, 615 (1975).
- [19] P. Armbruster *et al.*, *Nucl. Instrum. Methods* **139**, 213 (1976).
- [20] W. Lang *et al.*, *Nucl. Phys. A* **345**, 34 (1980).
- [21] U. Quade *et al.*, *Nucl. Phys. A* **487**, 1 (1988).
- [22] S. Julien-Laferrrière *et al.*, *Phys. Rev. C* **102**, 034602 (2020).
- [23] U. Quade *et al.*, *Nucl. Instrum. Methods* **164**, 435 (1979).

- [24] J. Bocquet, R. Brissot, and H. Faust, *NIM A* **267**, 466 (1988).
- [25] J. Bocquet and R. Brissot, *Nucl. Phys. A* **502**, 213 (1989).
- [26] H. G. Börner and F. Gönnenwein, *The Neutron: A Tool and an Object in Nuclear and Particle Physics* (World Scientific, Singapore, 2011), Chap. 4.
- [27] P. Egelhof, in *Advances in Solid State Physics 39*, edited by B. Kramer (Springer, Berlin, 1999), pp. 61–76.
- [28] P. Egelhof and S. Kraft-Bermuth, *Top. Appl. Phys.* **99**, 469 (2005).
- [29] S. Kraft-Bermuth *et al.*, *Rev. Sci. Instrum.* **80**, 103304 (2009).
- [30] A. Echler *et al.*, *Nucl. Instrum. Methods Phys. Res., Sect. B* **391**, 38 (2017).
- [31] S. Dubey *et al.*, *J. Low Temp. Phys.* **193**, 1257 (2018).
- [32] S. Dubey *et al.*, *EPJ Web Conf.* **193**, 04002 (2018).
- [33] *The Nuclear Fission Process*, edited by C. Wagemans (CRC, Boca Raton, FL, 1991).
- [34] H. G. Clerc *et al.*, *Z. Phys. A: At. Nucl.* **274**, 203 (1975).
- [35] C. Schmitt *et al.*, *Nucl. Phys. A* **430**, 21 (1984).
- [36] S. Dubey, A. Echler, P. Egelhof, P. Grabitz, W. Lauterfeld, M. Mutterer, S. Stolte, A. Blanc, U. Köster, O. Serot, G. Kessedjian, S. Kraft-Bermuth, P. Scholz, and F. Gonnwein, *Phys. Rev. C* **102**, 044602 (2020).
- [37] P. Egelhof *et al.*, report, Institut Laue-Langevin (ILL) (2015), doi: [10.5291/ILL-DATA.3-01-646](https://doi.org/10.5291/ILL-DATA.3-01-646).
- [38] Y. K. Gupta, D. C. Biswas, O. Serot, D. Bernard, O. Litaize, S. Julien-Laferrrière, A. Chebboubi, G. Kessedjian, C. Sage, A. Blanc, H. Faust, U. Köster, A. Ebran, L. Mathieu, A. Letourneau, T. Materna, and S. Panebianco, *Phys. Rev. C* **96**, 014608 (2017).
- [39] S. Julien-Laferrrière, Approche expérimentale et phénoménologique des rendements de la fission induite par neutron thermique du ^{239}Pu et du ^{241}Pu , Ph.D. thesis, Université Grenoble-Alpes, 2018.
- [40] S. Julien-Laferrrière *et al.* (unpublished).
- [41] G. Diiorio and B. Wehring, *Nucl. Instrum. Methods* **147**, 487 (1977).
- [42] A. Göök, F.-J. Hamsch, and S. Oberstedt, *EPJ Web Conf.* **239**, 05009 (2020).
- [43] M. Albertsson, B.G. Carlsson, T. Dossing, P. Moller, J. Randrup, and S. Aberg, *Phys. Rev. C* **103**, 014609 (2021).
- [44] B. L. Tracy *et al.*, *Phys. Rev. C* **5**, 222 (1972).
- [45] A. C. Wahl, *J. Radioanal. Chem.* **55**, 111 (1980).
- [46] H. Nifenecker *et al.*, *Z. Phys. A: At. Nucl.* **308**, 39 (1982).
- [47] S. Steinhäuser *et al.*, *Nucl. Phys. A* **634**, 89 (1998).
- [48] F. Rejmund *et al.*, *Nucl. Phys. A* **678**, 215 (2000).
- [49] B. Jurado and K.-H. Schmidt, *J. Phys. G: Nucl. Part. Phys.* **42**, 055101 (2015).
- [50] U. Köster, H. Faust, T. Materna, and L. Mathieu, *Nucl. Instrum. Methods Phys. Res., Sect. A* **613**, 363 (2010).